Not to appear in Nonlearned J., 45.

High temperature combustion: Approaching equilibrium using nuclear networks

R.M.Cabezón, D. García-Senz[1] and E. Bravo[1]

Departament de Física i Enginyeria Nuclear, UPC, Jordi Girona 3, Mòdul B5, 08034 Barcelona, Spain

ruben.cabezon@upc.es domingo.garcia@upc.es eduardo.bravo@upc.es

ABSTRACT

A method for integrating the chemical equations associated with nuclear combustion at high temperature is presented and extensively checked. Following the idea of Müller (1986), the feedback between nuclear rates and temperature was taken into account by simultaneously computing molar fraction changes and temperature response in the same matrix. The resulting algorithm is very stable and efficient at calculating nuclear combustion in explosive scenarios, especially in those situations where the reacting material manages to climb to the nuclear statistical equilibrium regime. The numerical scheme may be useful not only for those who carry out hydrodynamical simulations of explosive events, but also as a tool to investigate the properties of a nuclear system approaching equilibrium through a variety of thermodynamical trajectories.

Subject headings: nuclear reaction networks, explosive nucleosynthesis- supernovae: general

1. Introduction

Explosive phenomena in stars are often associated with the rapid release of nuclear energy and a lavish production of nuclear species. In any calculation dealing with novae or supernovae explosions it is highly desirable to implement the nuclear part of hydrodynamic

[1]Institut D'Estudis Espacials de Catalunya, Gran Capità 2-4 08034 Barcelona

codes as better as possible in order to get a suitable representation of these explosions and nucleosynthetic yields. A complication arises because of the huge quantity of nuclei involved, which makes it difficult to simultaneously handle hydrodynamics and nuclear combustion. Recently, however, there have been performed hydrodynamic simulations in spherical symmetry incorporating several thousand nuclei (Rauscher et al. 2001). Also, calculations in two or three dimensions of both kinds of supernovae are quite common. In these multidimensional calculations the mission of the nuclear network is to provide a reasonable nuclear energy rate at a minimum computational cost. This is usually accomplished by using small networks of 7 or 13 isotopes (Timmes, Hoffman & Woosley 2000). Detailed nucleosynthesis is calculatedted *a posteriori* by using a postprocessing technique with a larger network.

The most common procedure used for integrating the nuclear networks handles the discretized chemical equations in their implicit form. This enhances the stability of the nuclear system, which is very rigid (Arnett 1996), allowing it to take longer time-steps. It is worthy of note that despite the great dependence of the rates on the temperature, the effect of the latter is rarely incorporated implicitly into numerical codes. This enforces to make a reliable extrapolation of the temperature and to take small time-steps to guarantee stability, especially when the nuclei approach the nuclear statistical equilibrium (NSE) regime. Several methods have been suggested for handling nuclear combustion around the NSE regime. The most simple and fastest way is to use a conventional integration method when the nuclear system is not too close to equilibrium and to rely on statistical techniques to treat the phase in which direct and reverse reactions are almost or completely balanced. Nevertheless, this leads to the problem of how to make a smooth transition between the two regimes. Another possibility is to always use a standard integration method, which takes care of adequately restricting the time-step near equilibrium. In this case the computational effort increases. There are also mixed schemes (Hix & Thielemann 1996) in which reduced networks are used to describe the evolution of light and a few intermediate-mass elements (generally below ^{28}Si or ^{32}S) and a statistical approach is taken for handling the remaining nuclei. While this method is a very promising tool for explosive nucleosynthesis studies, due to its ability to handle hundreds of nuclei with a low computational burden, the decoupling between the thermal evolution and nuclear kinetics again imposes a constraint on time-steps near NSE.

The importance of solving the nuclear network by coupling molar fractions and temperature in the same matrix was demonstrated by Müller(1986), who used a small network of 13 nuclei, from helium to nickel. He showed how the inclusion of the temperature effects was decisive in avoiding the numerical oscillations which otherwise appear during and after relaxation to the NSE regime. However, in that paper there were presented only very few test calculations, limited to isochoric combustion. Moreover, the use of an entropy equation instead of the most frequently used energy equation was preferred to calculate the temperature

evolution.

In this paper we extend Müller's previous work to consider a larger nuclear network and to analyze in greater detail the transition between time-dependent combustion to complete nuclear equilibrium and viceversa. We also propose a method for integrating based on the energy equation that is robust and straightforward to implement, giving very good results in all the realized tests. In addition we have exhaustively checked our numerical scheme against a large variety of thermodynamic conditions of astrophysical interest. These include not only isochoric combustion, as considered in Müller seminal work, bul also adiabatic, isothermal and isobaric processes, as well as the particular case of combustion within a strongly coupled coulombic plasma.

Nowadays the effort to write the proposed numerical scheme for larger networks (even of 'kilo-nuclide' size) is considerably less than a decade ago, as we have the great advantage of a recently published library of theoretical reactions rates (i.e. Rauscher & Thielemann 2000 or the NACRE compilation, Angulo et al. 1999). An efficient algorithm of this kind could be suitable for handling a variety of vigorous nuclear combustion modes such as detonation, flames or silicon photodisintegration. It is especially useful whenever the operator splitting technique has to be applied to save computational time. Currently, this often happens in hydrodynamic calculations of both kinds of supernovae; in these situations the implicit thermal coupling could help to enlarge the time-steps without degrading neither the accuracy nor the stability of the system. There is also the additional advantage to this scheme that it is more compatible with the philosophy behind the post-processing technique. A necessary condition for obtaining a detailed nucleosynthesis from the thermal history of an explosive event, calculated beforehand using a reduced network, is that the small and large networks give a similar energy release. Integrating the chemical equations along with the energy conservation helps to fulfill this requirement.

In § 2 we describe the method of calculation and its implementation in two nuclear networks with 14 nuclei and 86 nuclei respectively. The ability of the scheme to monitor the quasi (QSE) and complete statistical equilibria is discussed. In § 3 the results of three tests are provided: adiabatic expansion from the NSE stage, hydrostatic and explosive silicon burning and nuclear flame propagation, all of them of evident interest to current studies on supernovae. The role of Coulomb corrections on the chemical composition of burned matter at high densities is also discussed in § 3. Finally, § 4 is devoted to summarizing the conclusions.

2. Method used for integrating the nuclear network

To integrate the set of differential equations associated with the nuclear species we have chosen a scheme based on the simple and well checked implicit method by Arnett & Truran (1969). The main motivation behind such election is that Arnett&Truran method has been traditionally used in nucleosynthetic calculations, always giving satisfactory results with low computational effort. In addition it is straightforward to modify in order to incorporate the thermal feedback and other proposed changes into the basic scheme. There are some differences between our integration method and that used in Müller(1986) worth to mention. In Müller's work the evolution of the system was followed by coupling the nuclear evolution with the entropy changes at constant density. Moreover, it was assumed that entropy changes were only due to the release of nuclear energy, thus no other sources of entropy were considered. Instead of the entropy equation our formulation uses energy conservation which is more often found in current calculations of explosive combustion. Moreover, the proposed algorithm is quite general, not restricted to isochoric processes, and potential entropy variations coming from heat exchange were also included. Minor effects, such as the incidence of coulombic corrections to the ionic component of the plasma and screening enhancement factors have been also incorporated to our scheme. A simplified description of our method can be found in García-Senz&Cabezón (2003).

Starting from a typical differential equation governing the evolution of the molar fractions of the i-specie, Y_i:

$$\frac{dY_i}{dt} = \sum_{k,l} r_{kl} Y_k Y_l - \sum_j r_{ij} Y_i Y_j + \sum_m \lambda_m Y_m - \lambda_i Y_i \tag{1}$$

where $r_{ij} = \rho \mathrm{N_A} < \sigma, v >_{ij}$ stands for particle reactions and λ_i is for photodisintegrations and decays. As usual, reaction rates between identical particles have to be divided by the corresponding factor (two or six for binary and ternary reactions respectively). The triple-alpha reaction was also incorporated to equations (1). Other possible three body reactions can be included in the same way. This set of equations is then linearized by taking

$$Y_i^{n+\theta} = Y_i^n + \theta \Delta Y_i \tag{2}$$

where Y_i is the molar fraction of the i-nuclei, n the integration step and $0 \leq \theta \leq 1$ a parameter which allows the quality of the integration to be controlled. Choosing $\theta = 1$ leads to a totally implicit first order integration; $\theta = 1/2$ is centered (second order) implicit and $\theta = 0$ is totally explicit. Then, neglecting the terms in $\Delta Y_i \cdot \Delta Y_j$, the linearized version

of the chemical equations is written. With the same level of accuracy we propose to take $T^{n+\theta} = T^n + \theta\Delta T$ and approximate the nuclear reaction rates by taking

$$r_{ij}(T^{n+\theta}) \simeq r_{ij}(T^n) + \frac{dr_{ij}}{dT}\Big]_{T^n} \theta\Delta T \tag{3}$$

If we also neglect second order terms in temperature, such as $\Delta Y_i \Delta T$, we can approximate a typical element on the right part of chemical equations (1) by:

$$Y_i^{n+1}\ Y_j^{n+1}\ r_{ij}(T^{n+1}) \simeq \left[Y_i^n\ r_{ij}(T^n)\right]\theta\Delta Y_j + \left[Y_j^n\ r_{ij}(T^n)\right]\theta\Delta Y_i + \left[Y_i^n\ Y_j^n \frac{dr_{ij}}{dT}\right]\theta\Delta T + Y_i^n Y_j^n r_{ij}(T^n) \tag{4}$$

then, equation (1) reads:

$$\frac{\Delta Y_i}{\Delta t} = +\sum_{k,l} r_{kl} Y_l^n \theta\Delta Y_k + \sum_{k,l} r_{kl} Y_k^n \theta\Delta Y_l - \left(\sum_j r_{ij} Y_j^n\right)\theta\Delta Y_i - \sum_j r_{ij} Y_i^n \theta\Delta Y_j + \sum_m \lambda_m \theta\Delta Y_m - \lambda_i \theta\Delta Y_i + \left(\sum_{k,l} r'_{kl} Y_k^n Y_l^n - \sum_j r'_{ij} Y_i^n Y_j^n + \sum_m \lambda'_m Y_m^n - \lambda'_i Y_i^n\right)\theta\Delta T + \sum_{k,l} r_{kl} Y_k^n Y_l^n - \sum_j r_{ij} Y_i^n Y_j^n + \sum_m \lambda_m Y_m^n - \lambda_i Y_i^n \tag{5}$$

Note that the derivative of nuclear rates with respect temperature, r'_{ij} and λ'_i, do not pose a practical problem since the recently published fitting formulae of Rauscher & Thielemann (2000) can be used to calculate them in an efficient way. Using that compilation through all stages of the combustion also leads to a complete internal coherence between direct and inverse rates when the equilibrium is approached, which is an essential condition for the proper handling of NSE.

For a network of N species we have N linear equations with $\mathrm{N}+1$ unknowns. An additional equation, energy equation, is needed in order to close the system. For a process not involving particle difussion it writes:

$$dQ = -P\frac{d\rho}{\rho^2} + \frac{\partial U}{\partial \rho}d\rho + \frac{\partial U}{\partial T}dT + \sum_i \left(-\mathrm{BE}_i + \frac{\partial U}{\partial Y_i}\right) dY_i \tag{6}$$

where P is pressure, U is the energy per gram of material, BE_i represents the nuclear binding energy of a mol of the i-species and dQ can also include sources or sinks of energy other than nuclear.

It is useful to write that equation by using the thermodynamical identity:

$$P = T\left(\frac{\partial P}{\partial T}\right)_{\rho} + \rho^2\left(\frac{\partial U}{\partial \rho}\right)_{T} \tag{7}$$

thus, using $T^{n+\theta} = T^n + \theta\Delta T$, the discretized form of the energy equation is easily written. For example, for an adiabatic process equation (6) reads:

$$\sum_i \left(\mathrm{BE}_i - \frac{\partial U}{\partial Y_i}\right)\Delta Y_i - \left\{\left(\frac{\partial U}{\partial T}\right)^n - \frac{\Delta\rho}{\rho^2}\left(\frac{\partial P}{\partial T}\right)^n \theta\right\}\Delta T = -T^n\frac{\Delta\rho}{\rho^2}\left(\frac{\partial P}{\partial T}\right)^n \tag{8}$$

for an ideal gas of ions $\partial U/\partial Y_i = (3/2)\mathrm{N_A kT}$, which is usually much lower than the Q-value of the reactions. Coulomb corrections to the ideal gas must be also included when the ionic coupling constant parameter, $\Gamma_i = 2.27\times10^5 < Z^{5/3} > (\rho\, Y_e)^{1/3}\, T^{-1}$, becomes non negligible. This often happens in high temperature combustion of degenerate matter because of the strong dependence of Γ_i on the mean charge of the system . Such dependence also favours $\partial U/\partial Y_i$ of the products of charged particle reactions against that of the reactant particles. Thus, on the whole, both contributions to $\partial U/\partial Y_i$ (ideal gas and Coulomb corrections) work in the same direction, slightly increasing the equilibrium temperature for a given density. Therefore, regardless the density regime we have *always kept* both contributions to $\partial U/\partial Y_i$ in equation (8).

Interestingly the implicit treatment of temperature also allows for the proper handling of quasi-hydrostatic and isobaric processes. Let's suppose that the value of the actual pressure of the system, P, remains always close to the external pressure, $\mathrm{P_{ext}}(t)$, so that $P = P_{ext} + dP$. Then, writing $dP = (\partial P/\partial T)dT + (\partial P/\partial\rho)d\rho + \sum_i(\partial P/\partial Y_i)dY_i$ and taken out $d\rho$ the energy equation (eq.[6]) reads:

$$\begin{aligned} dQ = \sum_i \left\{-\mathrm{BE}_i + \left(\frac{\partial U}{\partial Y_i}\right) + \frac{T}{\rho^2}\left(\frac{\partial P}{\partial T}\right)\left(\frac{\partial P}{\partial Y_i}\right)\left(\frac{\partial P}{\partial \rho}\right)^{-1}\right\} dY_i + \\ \left\{\left(\frac{\partial U}{\partial T}\right) + \frac{T}{\rho^2}\left(\frac{\partial P}{\partial T}\right)^2\left(\frac{\partial P}{\partial \rho}\right)^{-1}\right\} dT - (P - P_{ext})\frac{T}{\rho^2}\left(\frac{\partial P}{\partial T}\right)\left(\frac{\partial P}{\partial \rho}\right)^{-1} \end{aligned} \tag{9}$$

Once this equation is discretized (in a similar way that we did for eq.[6]) and solved jointly with equations (5) the solution, ΔT and ΔY_i, can be used along with P_{ext} to find $\Delta\rho$. Equation (9) has been used in §3.3 to solve the structure of a nuclear flame.

From here on we will focus on the case of $\theta = 1$ which is expected to give the most stable system behaviour of the nuclear system. A recalculation of the first test presented in the next section with $\theta = 0.5$ did not lead to relevant quantitative changes in the results. The standard criterion to assign the integration time-step was to demand that the fractional change in temperature and molar fractions of the more abundant species would not exceed 2% per model. Nevertheless, one can safely relax that criterion even to 10-15% variation in molar fractions without seriously modify the quantitative results.

This set of linear equations can be efficiently solved by using standard sparse matrix algorithms. We in particular used the one found in Prantzos, Arnould & Arcoragi (1987). The resulting algorithm led to a satisfactory mass conservation, the error in the sum of mass fractions was always lower than 10^{-10}, close machine precision, for the calculations described in §3. There is not a large loss of computational efficiency when the linearized thermal coupling is turned on. The main source of degradation of that type is the computation for the derivatives of the rates rather than the increase in the size of the matrix from $\{N \times N\}$ to $\{(N+1)\times(N+1)\}$. From the tests carried out we estimate that our numerical treatment leads to a time overload under 15% and 2% for the 14 and 86-nucleus systems respectively. Several tests were run which demonstrated the ability of the scheme to monitor rapid isochoric combustion followed by adiabatic expansion in the hydrodynamic time scale. Adding either diffusive terms or those related to the artificial viscosity formulation to the right side of equations (6) and (9) allows us to include heat transport and shock wave heating in the scheme. An extreme case of heat transport, the propagation of a nuclear flame, is also presented and checked in § 3. Even though all the test presented below were calculated solving the linearized equations (5) and (8) an improvement of the algorithm based on the iterative refinement of the solution is also given and discussed in §3.1.2.

3. Testing the algorithm

Three test cases were calculated in order to check the method. All of them are of an indisputable interest in explosive combustion: a) isochoric combustion followed by adiabatic expansion once complete NSE has been achieved, b) endoenergetic disintegration of silicon and c) isobaric nuclear flame propagation.

The nuclear network consists of 86 nuclei spanning from ^{12}C to ^{60}Zn including α, p and

n particles, as depicted in Figure 1. Even though this is not a large network, but rather a moderate one, it is certainly more complex than the α-chain considered in Müller (1986). On another note, to avoid an excessive computational burden, current multidimensional simulations of supernovae can only support very reduced networks. For this reason, we also carried out several runs of the test using an α-network of 14 nuclei, a subset of the previous sample of 86 nuclei. This reduced set was similar to the sets of 7 and 13 nuclei considered in the comparative study about the performance of small nuclear networks carried out by Timmes et al. (2000) . Nuclear rates on light elements ,up to ^{20}Ne, were taken from Caughlan & Fowler (1988), and from Rauscher & Thielemann (2000) above neon.

A common feature of all the tests shown here is that nuclear burning proceeds through the so-called e-process, thus it manages to achieve complete nuclear equilibrium at high temperature. In nature, that equilibrium does not last very long because it is cut by the reduction in density as the expansion progresses. At some point the temperature becomes too low to allow the nuclear reactions to proceed and the chemical abundances freeze out. The precise value of the resulting abundances is a function of the initial entropy of the material in the NSE phase, the degree of neutronization of the material and the rate of the expansion, as many studies have demonstrated (see for instance Meyer, Krishnan & Clayton 1998 for a recent work and references therein).

The equation of state (EOS) used in all the tests was quite complete, consisting of a mix of electrons treated as a partially degenerate relativistic gas, an ideal gas of ions with Coulomb and other minor corrections, and radiation. Although important at high densities, electron capture on protons and nuclei have not been included in these calculations. Nevertheless, they can be incorporated into the scheme with the same formulation expressed in equations (2) and (3).

The treatment of electrostatic corrections deserves further discussion. At high densities the energy of the plasma deviates from that of a pure ideal gas of nuclei and electrons. Electrostatic interactions must be taken into account in this regime, even in NSE, owing to the strong dependence of such interactions with the average charge of the system. The electrostatic energy of the k-specie associated to the Coulomb interactions, U_k^C (erg. g^{-1}), can be approximated by the following expressions (Ogata & Ichimaru 1987, Yakolev & Shalybkov 1987):

$$\frac{U_k^C}{\mathrm{N_A kT} Y_k} = \begin{cases} a\Gamma_k + b\Gamma_k^{\frac{1}{4}} + c\Gamma_k^{-\frac{1}{4}} + d & \Gamma_k \geq 1 \\ -\frac{\sqrt{3}}{2}\Gamma_k^{\frac{3}{2}} + \beta\Gamma_k^{\gamma} & \Gamma_k < 1 \end{cases} \tag{10}$$

where Γ_k is the ionic coupling constant parameter of the k-nuclei, a=-0.8980, b=0.96786,

c=0.2207, d=-0.86097, $\beta = 0.29561$ and $\gamma = 1.9885$. The chemical potentials, μ_k^C, can be easily derived from expression (10). Nevertheless, the inclusion of Coulombic interactions affects not only the thermodynamics, they also slightly alters the rates of electron captures and the rate of nuclear reactions through the corresponding screening factors. As we have not included weak interactions in the network we will not address the first point. The second point, the incorporation of screening corrections to the nuclear rates in the scheme should be straightforward. However, there is also necessary to compute the derivatives of such corrections with respect to temperature, as we did with the nuclear reaction rates.

In the following, we are mainly interested in the behaviour of the system when it approaches the NSE. In this case it is enough to make a simplified treatment of the screening. In particular, we take the enhancement factors given by Mochkovitch & Nomoto (1986) who, among other things, studied the equilibrium of direct and reverse reactions when strong screening corrections are taken into account. They found that the dominant term in the enhancement factor, EF, to direct capture reactions is:

$$\mathrm{EF} = \exp\left[\frac{\Delta\mu^C}{kT}\right] \tag{11}$$

where $\Delta\mu^c$ is the chemical potential of the reactants minus that of the products. The above expression is especially adequate for non-resonant reactions at high temperature as well as for resonant reactions with large enough resonance energy. Note that, in this approximation the use of the enhancement factors given by equation (11) does not affect to the photodisintegration reactions calculated through the detailed balance, because the Q-value of the reaction becomes $Q \rightarrow Q_0 + \Delta\mu^C$ which exactly compensates the screening correction. In the limit of complete nuclear equilibrium this approach leads to the same results as the statistical description given by the Saha equation with the chemical potentials corrected for electrostactic interactions (Bravo& García-Senz 1999).

3.1. Isochoric combustion and further expansion

Isochoric combustion is a very interesting test because the original fuel (usually helium or carbon and oxygen in many explosive events) goes through several modes of burning: initial fast burning followed by quasi-statistical and complete nuclear equilibrium. Further expansion will take the combustion out of NSE, which leads to a rapid freezing of the abundances. In hydrodynamic calculations, that regime might be associated to a detonation wave passing through degenerate material.

To begin, the combustion of a system composed of equal parts ^{12}C and ^{16}O at $\rho = 10^9$ g.cm^{-3} was followed *without* including the implicit coupling between abundances and temperature. The result is shown in Figure 2, where we can see that mass fractions begin to *oscillate* as soon as the combustion approaches the equilibrium regime. This behavior is characteristic of any stiff system of differential equations solved with explicit rather than implicit schemes, demanding very short time-steps to control the system ($< 10^{-9}$ s). The evolution *with* thermal coupling is depicted in Figure 3; here the oscillations *did not show up* and the QSE and NSE regimes were handled without problems, despite the large time-steps ($\simeq 0.1$ s, even larger than the hydrodynamic timescale τ_{HD}, see below) taken once equilibrium was achieved. From Tables 1 and 2 we can see that the most abundant nuclei correspond to Fe-peak elements, especially ^{54}Fe (27%, in mass) and also to helium (almost 20%). Such abundances and the high temperature achieved during the isochoric combustion are in agreement with the current picture of NSE (Arnett 1996).

The integration scheme also allowed us to follow a rapid adiabatic expansion in the hydrodynamic timescale $\tau_{HD} = 446/\sqrt{\rho}$ s immediately after the NSE regime was reached:

$$\rho(t) = \rho_0 \ \exp[-t/\tau_{HD}] \tag{12}$$

During the expansion there was no need to impose any particular freeze-out temperature for the nucleonic system. In Table 1 we provide the mass fractions at five different fiducial temperatures achieved along the cooling path. From these numbers we can see that there is a large spread in the freezing temperatures. Many species are still changing even below $T = 2 \times 10^9$ K, although their abundances are generally too low to be significative. The most abundant element, ^{56}Ni, freezed around $T \simeq 3 \times 10^9$ K which is not a high enough temperature to keep the NSE going. Thus, whenever the Saha equation is used to describe nuclear statistical equilibrium above $4 - 5 \times 10^9$ K one has to be cautious and switch to a time-dependent network calculation below that critical temperature because the material is not completely burned yet.

In Table 2 we provide the freeze-out temperature and final composition for each of the five most abundant nuclei as a function of the initial thermodynamical state and chemical composition. As one can see, while the critical temperature for achieving complete NSE was the same for all nuclei this was certainly not true for the freeze-out temperature. When the initial fuel was composed of carbon and oxygen with no neutron excess, $\eta = 0$ ($\eta = 1 - 2Y_e$), the resulting abundances were largely dominated by ^{56}Ni. Under the conditions of our numerical experiment, ^{56}Ni froze at $T_9 = 3.28$, while other Fe-peak isotopes were still reacting with residual protons and neutrons. Therefore their freezing temperatures were lower. A similar calculation (same initial density and temperature) is shown in the second row of

Table 2, but the initial composition was 30% ^{12}C, 30% ^{16}O and 40% ^{22}Ne, resulting in a moderate neutron excess of $\eta = 0.0364$. This time the dominant nucleus after the adiabatic cooling was not ^{56}Ni but instead were ^{54}Fe and ^{58}Ni in accordance with well-known results (i.e., Clayton 1968). There is, however, a clear difference in the freezing temperatures of these dominant isotopes.

The third row of Table 2 and Figure 4 summarizes the evolution of a system initially composed of pure helium at $\rho = 4 \times 10^6$ g.cm^{-3}. In this case $\eta = 0$ and the combined value of temperature and density in NSE resulted in a larger entropy than in the two earlier cases. Now, the period of relaxation to NSE was larger than in the two precedent tests; however there was no sign of instability during the integration. Once the NSE was achieved, at $T = 4.3 \times 10^9$ K, the composition was again dominated by Fe-peak elements with a lower concentration of light particles α and p, (0.66% and 0.74% by mass respectively) than in the two precedent cases. For a given initial density the outcome of the adiabatic cooling depends on the adopted expansion rate. For very fast expansions the alpha particles have some difficulty to react, owing the low-density environment, and the final distribution is rich in α particles and intermediate-mass elements (Woosley, Arnett & Clayton 1973). In our calculation the expansion rate was not rapid enough to allow the synthesis of intermediate-mass elements in appreciable amounts. According to Table 2 the final composition was completely dominated by ^{56}Ni (98%) and Fe-peak elements plus a little amount of unburnt helium.

3.1.1. Influence of screening factors in the equilibrium distribution of nuclei

As mentioned above, the enhancement factors to the nuclear reaction rates given by equation (11) were taken into account in all the realized tests. Generally speaking, their inclusion in explosive processes, although important, is not very crucial; its main effect being to shift the temporal evolution and the maximum value achieved by temperature. Therefore, there is expected to be some changes in the mass fractions of the species in NSE when screening factors are incorporated into the scheme, especially at high density. In Figure 5 there is represented the evolution of temperature during the isochoric combustion of a 50%-50% mix of carbon and oxygen at constant density of 4×10^9 g.cm^{-3}. As we can see the profiles with and without enhancement factors are not very different, although the induction time is shorter and the equilibrium temperature is no longer the same: $T_9 = 9.51$ (no screening included) and $T_9 = 9.77$ (screening included). Again, there is a stable numerical behaviour of the system when the equilibrium is approached.

To analyze the nucleosynthesis during the NSE stage it is more convenient to compare

at the same temperature. In doing that not only the comparison among abundances becomes more reliable, but a direct check with the results obtained by using the nuclear Saha equation with the mass excesses corrected from the coulombic part of the chemical potentials deduced from equation (10) is also possible. The results of such comparison for the 14-nuclei network are depicted in Figure 6. From that figure it becomes clear that the main effect of screening corrections is to shift the distribution of the species towards higher atomic masses and that, the larger the density the bigger the change. In fact, the change in the NSE distribution of the nuclei depicted in Figure 6 looks rather spectacular. This is in part due to the limited size of the 14-nuclei chain; when the same calculation was repeated with the 86-nuclei network such differences were *spread out and smoothed*. For example, at $T_9 = 9.32$, $\rho_9 = 4$ the mean molecular weight calculated from the α-network was $\mu_i = 11.04$ g.mol^{-1} (no screening factors) and $\mu_i = 14.35$ g.mol^{-1} (with screening factors) whereas the corresponding values for the 86-nuclei network were $\mu_i = 10.54$ g.mol^{-1} and $\mu_i = 11.87$ g.mol^{-1} respectively. The comparison between the resulting mass fractions calculated through the network and the nuclear Saha equation also confirms that the adequate way to handle the coulombic interactions in the NSE regime is by substracting the electrostatic chemical potentials from the nuclear mass excesses (Bravo&García-Senz 1999).

3.1.2. Iterative refinement and accuracy

The integration scheme developed in § 2 can be considered as the first iteration step of a more general Newton-Raphson based method for solving the full non-linear equations governing the evolution of the nuclear system. When using these methods there is often an enhancement of the computational efficiency despite that the time invested per model is larger. In addition they also have the advantage that a check on accuracy is possible, allowing for a more consistent choice of the time-steps (Timmes 1999). Fortunately it is straightforward to modify our numerical scheme, with minimum changes, in order to allow the iterative refinement of the solution, as described below. The resulting algorithm is equivalent to the standard implicit multidimensional Newton-Raphson calculation. For a given $n+1$ time-step the iterative process leads to a sequence of 'solutions' $(Y_i^{n+1})^k$ and $(T^{n+1})^k$ for the i-specie and temperature which, after m iterations, should converge to the true values for Y_i^{n+1} and T^{n+1}. We define a set of functions G_i^0, which represents the discretized form of the chemical equations (1):

$$G_i^0[(\mathbf{Y}^{n+1})^k, (T^{n+1})^k] = F_i[(\mathbf{Y}^{n+1})^k, (T^{n+1})^k]\ \Delta t - [(Y_i^{n+1})^k - Y_i^n] \qquad k = 1...m \qquad (13)$$

where $(\mathbf{Y}^{n+1})^k = \{(Y_1^{n+1})^k ....(Y_N^{n+1})^k\}$ and F_i are the terms on the right of equation (1). A similar function ,G^1, representing the energy equation (8) is also defined:

$$G^1[(\mathbf{Y}^{n+1})^k, (T^{n+1})^k] = \sum_i \left(\mathrm{BE}_i - \frac{\partial U}{\partial Y_i} \right) [(Y_i^{n+1})^k - Y_i^n)] - \left\{ \left(\frac{\partial U}{\partial T} \right) - \frac{\Delta\rho}{\rho^2} \left(\frac{\partial P}{\partial T} \right) \right\} [(T^{n+1})^k - T^n] + T^n \frac{\Delta\rho}{\rho^2} \left(\frac{\partial P}{\partial T} \right) \tag{14}$$

The Newton-Raphson iterative method demands that $\delta G_i^{0,1} = -G_i^{0,1}$, which allows to solve for the corrections $\Delta Y_i, \Delta T$ to the approximate values $(Y_i^{n+1})^k$ and $(T^{n+1})^k$ found in the latest iteration. In this case the Jacobian matrix associated to $\delta G_i^{0,1}$ is *exactly the same* as the matrix of the linear system associated to equations (5) and (8). For the first iteration we take $(Y_i^{n+1})^1 = Y_i^n$ and $(T^{n+1})^1 = T^n$ so that when m=1 the extended Arnett&Truran method given by equations (5) and (8) is recovered. For $m > 1$ an iterative sequence results which usually ends when the k-corrections ΔY_i^k to $(Y_i^{n+1})^{k-1}$ and ΔT^k to $(T^{n+1})^{k-1}$ becomes negligible or, better, when the $G_i^{0,1}$ functions defined by equations (13) and (14), conveniently normalized, go to zero (for example we took $|G_i^0|/\sqrt{(F_i\Delta t)^2 + \Delta Y_i^2} < 5 \times 10^{-6}$ and a similar expression for G^1) . Usually convergence is achieved in 3-4 iterations. The criterion to choose the time-step was not very restrictive, we allowed for a 1.5% relative variation in temperature and 10% in molar fractions. In Figure 7 there is shown the evolution of the errors in mass fractions of several species during the isochoric carbon combustion, estimated by comparing the size of the corrections given by the first iteration with the algebraic sum of the lowest-order corrections given by the remaining iterations. As we can see in that figure the first iteration always led to a much larger correction, usually of two orders of magnitude or more, than that of the sum of the remaining iterations. Thus, the evolution of the mass fractions and temperature can reasonably be described taking only one iteration and neglecting second and higher-order corrections. For this particular test, a further relaxation of the criterion that restrict the time step led to several negative abundances. Nevertheless, the iterative Newton-Raphson scheme would also be in trouble in this case, due to the lack of convergence. Therefore, taking only one iteration along as a moderate time-step would generally be enough, especially if we are mainly interested in the thermal evolution of the system and in the gross features of the nucleosynthesis. For larger time-steps or for detailed nucleosynthetic studies it is better to rely on the iterative scheme which has the additional advantage that a check of the accuracy is feasible (Timmes 1999).

3.2. Hydrostatic and explosive silicon burning

Hydrostatic combustion of silicon is a quasi-equilibrium process from the beginning due to the important role played by photodisintegration reactions. One goal of this calculation is to check the ability of our integration scheme to describe silicon photodissociation at constant temperature and density. We also studied explosive silicon burning within an expanding medium, until the reactions were totally quenched. In both cases we compared our results with those of Timmes et al. (2000), which were calculated under the same environmental conditions. Thus, a system composed of 100% ^{28}Si at T=6×10^9K and $\rho = 10^7$ g.cm^{-3} was considered. In the hydrostatic case, the temperature was kept constant, therefore the feedback between nuclear kinetics and thermal evolution no longer took place. Nevertheless, our scheme was also able to keep track of this limiting case without introducing any modification. Instead to rewrite our code to not include ΔT terms in the matrix we have artificially raised the value of the specific heat during the silicon dissociation to keep the temperature constant. In the adiabatic expansion test the specific heat was again restored to its real value.

The results of these calculations for the small network are shown in Figures 8,9 and 10. A comparison between the evolution of the nuclear energy generation rate, provided in Figure 8, with respect to that shown in Figure 1a of Timmes et al. (2000) is satisfactory. The main difference is the tiny bump shown around t$\simeq 2\times10^{-4}$ s, which was probably due to the different libraries used to compute the nuclear rates. A comparison of their abundances (their Fig. 1c) with ours (Fig. 9) also shows a good agreement.

As a second check a piece of pure silicon was enforced to follow an adiabatic expansion in the hydrodynamic timescale as shown in equation (12). In this case, the temperature evolution was calculated self-consistently from the network. The results of this calculation for our $\alpha-$chain are summarized in Figures 8 and 10. These figures can be compared with Figures 2a,2c in Timmes et al. (2000), in which the temperature is evolved with an approximate analytical formula. The evolution of the nuclear energy rate follows a close path in both calculations. The comparison between abundances is also quite satisfactory, although there are divergences above t=0.1 s, which is about the hydrodynamical time τ_{HD}. These differences probably arise from the slightly different path followed by temperature in both calculations. We note that Timmes et al. (2000) only included the contribution of the radiation to the specific heat thus, for a given density, we found a higher value of temperature. In particular, our final silicon group abundance (up to titanium) was about five times higher than theirs. On the whole its composition is characteristic of an $\alpha-$rich freeze-out with a large abundance of ^{56}Ni (92% in mass) followed by ^{4}He (7%).

3.3. An example of isobaric combustion: The propagation of a subsonic nuclear flame

Thermonuclear flame propagation is a subsonic mode of energy propagation which takes place under nearly isobaric conditions. Flames could appear due to the combination of sharp thermal gradients, high conductivity and potentially explosive fuels such as helium or carbon and oxygen. These requirements may be fulfilled in the interior of those massive white dwarfs that are reactivated by the accretion from a companion star, giving rise to a Type Ia supernova. This calculation is more complex than those carried out in the previous subsections because both, the temporal evolution and the spatial structure of the flame have to be solved. Therefore our nuclear subroutine was coupled to the diffusion equation within an initially uniform grid of shells representing a physical system with planar geometry and constant density. Given the adequate initial conditions (see below), the advance of the flame was calculated directly from the nuclear network of 86 isotopes along with the isobaricity assumption (Timmes & Woosley 1992). A diffusive term was added to the energy equation so that the heat is transported from the burned to the unburned zone, mainly by electronic conduction. Thus, we take,

$$dQ = \dot{\mathrm{S}}_{dif}\ dt = \frac{1}{\rho}\nabla \cdot (\sigma \nabla \mathbf{T})\ dt \tag{15}$$

in equation (9) and set P_{ext} = constant in the same equation in order to keep the pressure constant during the flame propagation. The conductivity, σ, was that of Khokhlov, Oran and Wheeler (1997) which includes electronic and radiative contributions to the opacity. As the dependence of conductivity on temperature is much lower than it is in nuclear reactions this new term, equation (15), can be added to the independent terms in the corresponding discretized version of equation (9) . In order to build a nuclear flame the left side of a tube containing equal parts of carbon and oxygen was incinerated at constant pressure until NSE was achieved. After a brief transitory period the heat exchange between the burned the and cold material gave rise to a steady planar flame that moved at a constant velocity through the fuel with constant density $\rho_{fuel} = 1.26 \times 10^8$ g.cm^{-3}. Behind the flame front the original fuel was rapidly transformed into intermediate-mass elements, especially silicon; the temperature rose to 6.1×10^9 K; and the density dropped to $\rho = 7.6 \times 10^7$ g.cm^{-3} to keep the pressure constant. Under these conditions the ashes were in QSE and began to slowly relax to complete equilibrium, as can be seen in Figure 11. During the total elapsed time (about 10^{-5} s) the nuclear system did not show any sign of instability. The stationary velocity of the flame front was $\mathrm{v}_{flame} = 4.8$ km.s^{-1}, which is about 50% higher than that obtained by Timmes & Woosley (1992) for the same density. Such discrepancy is well within the factor two error usually attributed to the input physics (conductivities, nuclear libraries and EOS).

4. Conclusions

Current standard integration methods for chemical equations encounter some difficulty when handling high temperature combustion near equilibrium. The reason for this is the extreme sensitivity of nuclear rates to the temperature, which makes it difficult to reach a time-independent situation (equilibrium) when using a time-dependent solver for equations that describe the evolution of molar fractions. Müller (1986) pointed out that the solution is to implicitly couple the equations that give abundance changes with those that describe energy or entropy evolution. A practical drawback of such a procedure is that the derivatives of the nuclear reaction rates have to be worked out at each iteration. Nowadays, however, very complete libraries are available, which detail nuclear reaction rates for many species with simple formulae (i.e. Rauscher & Thielemann 2000). From these, then, derivatives can be evaluated without causing excessive computational overload.

The main purpose of this study was to build and check an integration method, inspired by Müller idea, that would be flexible enough to accommodate a variety of combustion modes involving quasi/total nuclear equilibrium at some point along the path of its evolution. Screening enhancement factors were also incorporated to our numerical scheme. Good astrophysical examples of the potential applicability of this algorithm would be for nuclear flames and detonation waves in Type Ia supernovae and for silicon burning in Type II supernovae respectively.

In spite of the simplicity of the proposed numerical algorithm, described in §2, we found that it was able to pass many tests related to high-temperature combustion, §3. In each of them stability was always preserved, even in the NSE stage, without restricting the time-step. The results also matched well those obtained in similar conditions by other authors using different integration schemes. A comparison of the numerical efficiency of the small chain (of 14 nuclei) and the moderate-sized one (of 86 nuclei) showed that the time overload introduced by thermal coupling was under 15%, and 2% for the small and large networks respectively. These factors arise mainly from the calculation of the derivatives of the nuclear rates rather than from the inversion of the matrix. Recently, the 14-isotope α-chain with thermal coupling was incorporated to a multidimensional SPH code designed to simulate Type Ia supernova explosions. In that situation, the average time degradation is far below the aforementioned 15% as the time expended per model is largely controlled by hydrodynamics, especially when one is searching for neighbours or calculating gravity.

The FORTRAN subroutines that implement the 14 α-chain and the 86-isotope network presented in this paper are made available by the authors to interested readers upon request.

This work was funded in part by MCYT grants EPIS98-1348 and AYA2000-1785; and CIRIT GRQ grants.

REFERENCES

Angulo C., et al., 1999, Nuc. Phys., A656,3

Arnett,D., 1996, Supernovae and Nucleosynthesis, (Princenton University Press)

Arnett, D.W., Truran, J.W., 1969, ApJ, 157, 339.

Caughlan, G.R., Fowler, W.A., 1988, Atomic Data and Nuclear Data Tables 40, 283.

Clayton, D.D., 1968, Principles of Stellar Evolution and Nucleosynthesis. (Chicago: Univ. Chicago Press).

Bravo, E., García-Senz, 1999, MNRAS, 307, 984

García-Senz, D., Cabezón, R.M., 2003, Nuc. Phys.A, 718, 566c.

Hix, W.R., Thielemann, F.-K., 1996, ApJ, 406, 869.

Khokhlov, A.M., Oran, E.S., Wheeler, J.C., 1997, ApJ, 478, 678

Meyer, B.S., Krishnan, T.D., Clayton, D.D., 1998, ApJ, 498, 808.

Mochkovitch, R., Nomoto, K., 1986, A&A, 154, 115

Müller, E., 1986, A&A, 162, 103.

Ogata, S., Ichimaru, S., 1987, Phys. Rev. A, 36, 5451

Prantzos, N, Arnould, M., Arcoragi, J.P., 1987, ApJ, 315, 209.

Rauscher T., Thielemann, F.-K., 2000, Atomic Data and Nuclear Data Tables 75, 1.

Rauscher, T., Heger, A., Hoffman, R.D., Woosley, S.E., 2001, Nuc. Phys.A, 688, 193c-196c.

Timmes, F.X., 1999, ApJS, 124, 241.

Timmes, F.X., Woosley, S.E., 1992, ApJ, 396, 649.

Timmes, F.X., Hoffman, R.D., Woosley, S.E., 2000, ApJS, 129, 377

Woosley, S.E., Arnett, W.D., Clayton, D.D., 1973, ApJS, 26, 231.

Yakovlev, D.G., Shalybkov, D.A., 1989, Soviet Sci.Rev.E, 7,311

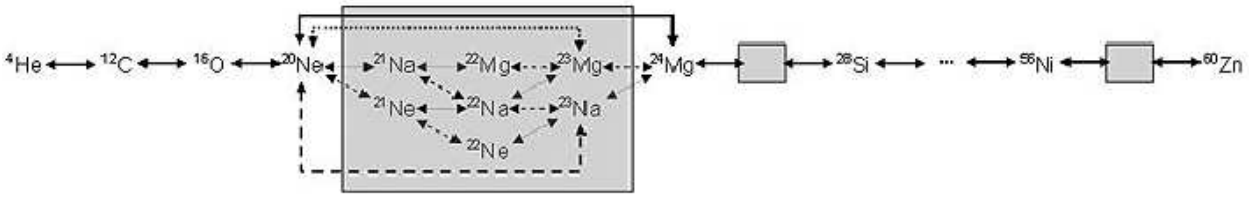

Fig. 1.— Sketch of the nuclear network used in the tests. It consists of 86 nuclei (including p, n and α particles), linked trough (p,γ) -thin solid arrows-, (n,γ) -small dotted arrows-, (α,γ) -thick solid arrows-, (α,p) -long dashed arrows-, and (α,n) -long dotted arrows-, as suggested by the plot. The network is organized into groups around an α-chain of 14 nuclei from ^{4}He to ^{60}Zn. One of these groups, between ^{20}Ne and ^{24}Mg, is shown in the figure. Triple alpha reaction and binary reactions of carbon and oxygen were also included.

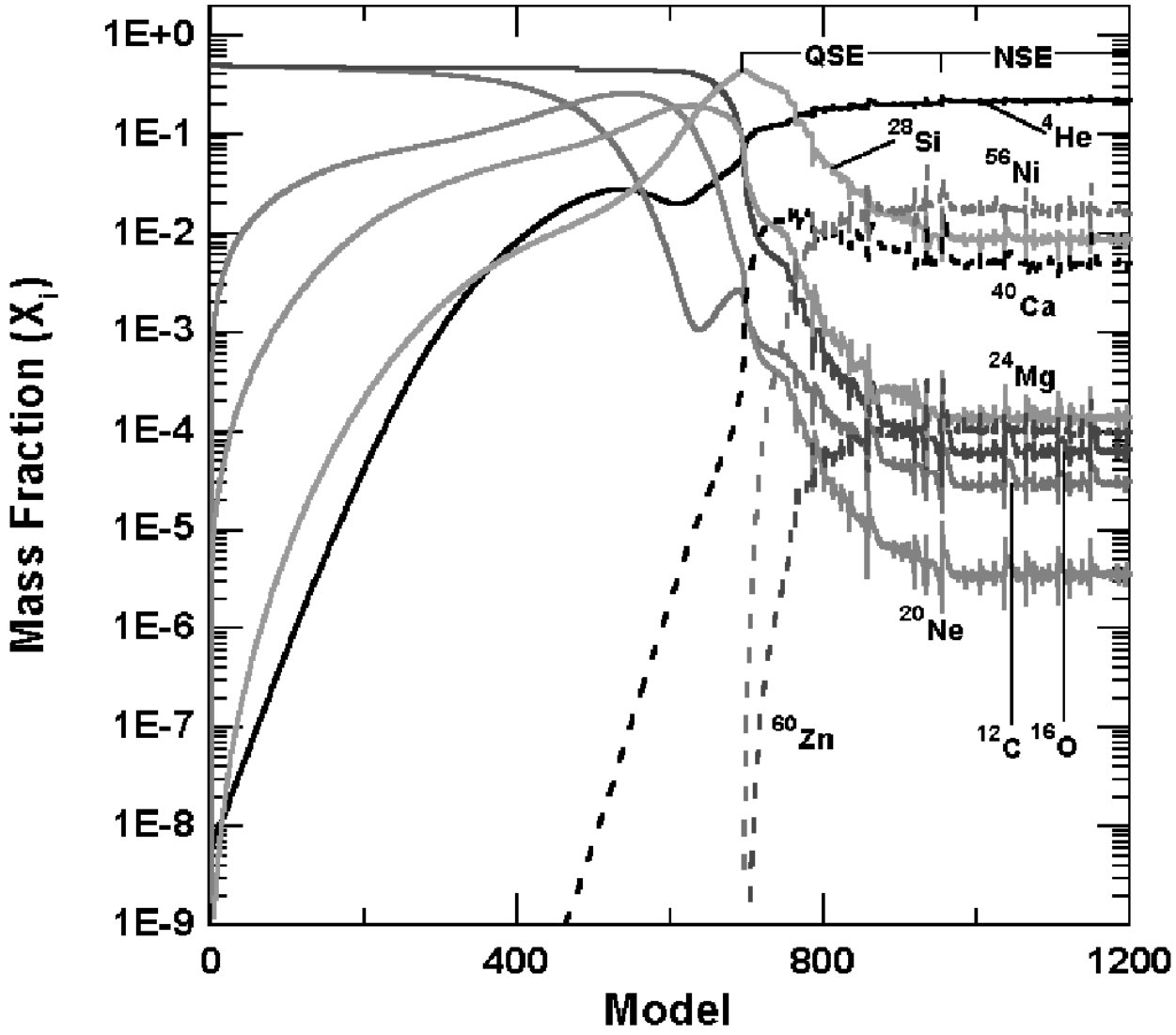

Fig. 2.— Evolution at constant density, $\rho = 10^9$ g.cm^{-3} of a 50% mix of carbon and oxygen calculated *without* implicit thermal coupling, the initial temperature was $T_0 = 10^9$ K. As soon as the combustion enters in the QSE zone and NSE plateau it becomes unstable (86-isotope network).

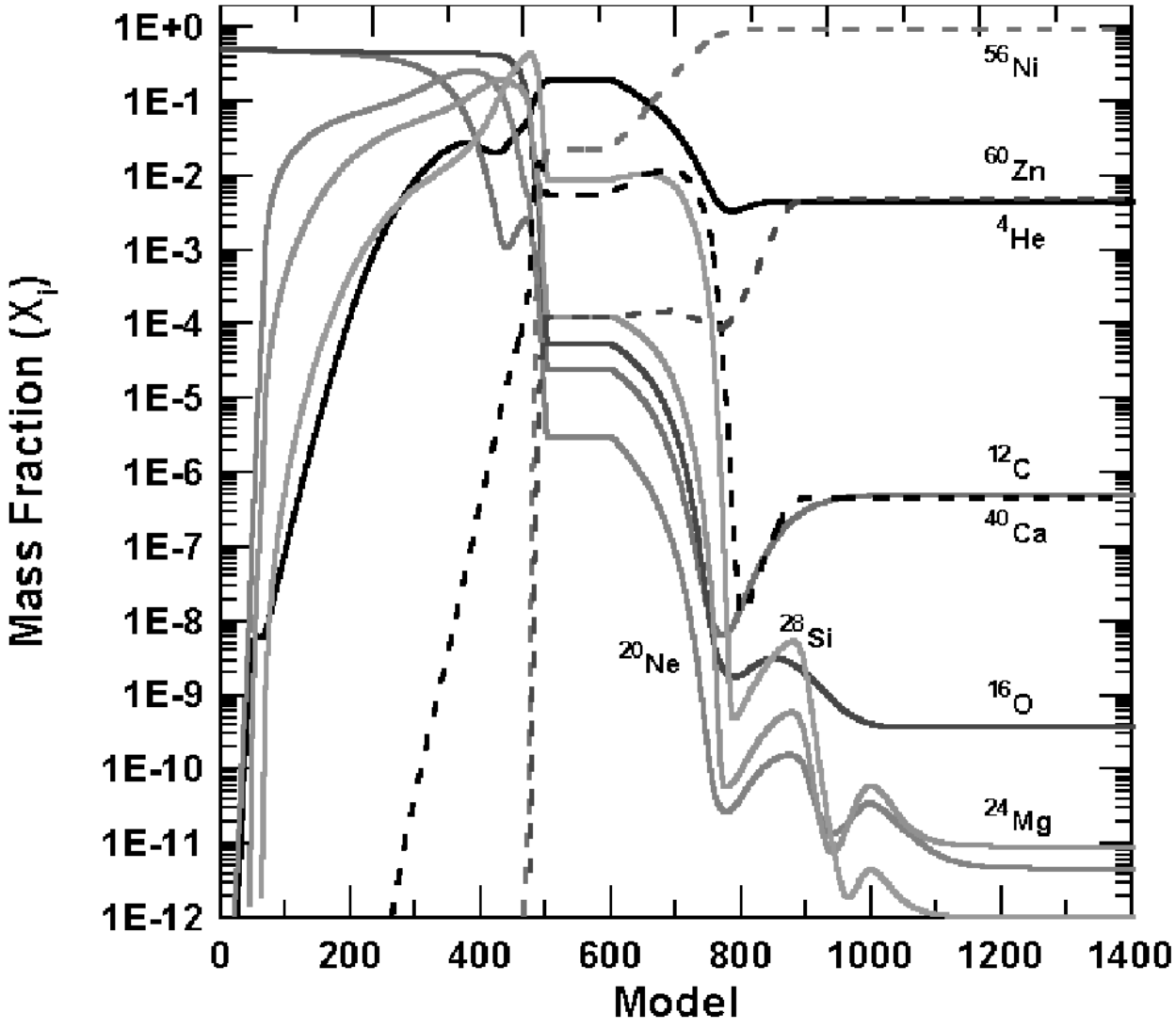

Fig. 3.— The same as in Figure 2, this time with the thermal coupling *turned on*. The system remains stable all the time. An adiabatic expansion was imposed above model 600 until all the nuclear reactions quenched (86-isotope network).

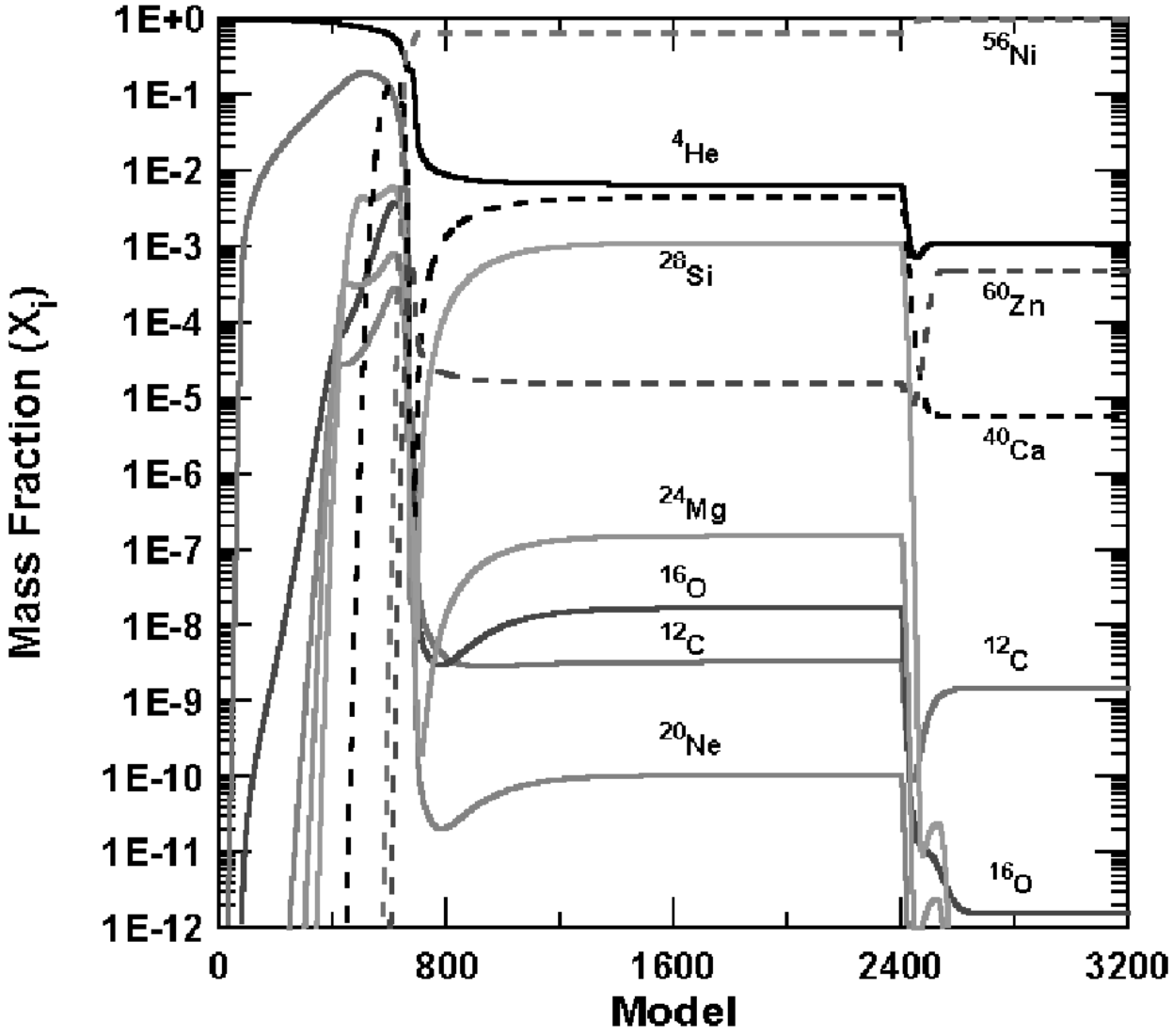

Fig. 4.— Isochoric combustion of pure helium (at $\rho = 4 \times 10^6$ g.cm^{-3}) followed by an adiabatic expansion in the hydrodynamic time. Owing to the lower ignition density it took more time for the combustion to reach complete equilibrium at T = 4.23×10^9 K. Nevertheless, the implicit thermal coupling again avoids any instability to grow. The resulting nucleosynthesis after the expansion is very rich in ^{56}Ni, with appreciable amounts of helium and minor concentration of α-elements such as ^{40}Ca (86-isotope network).

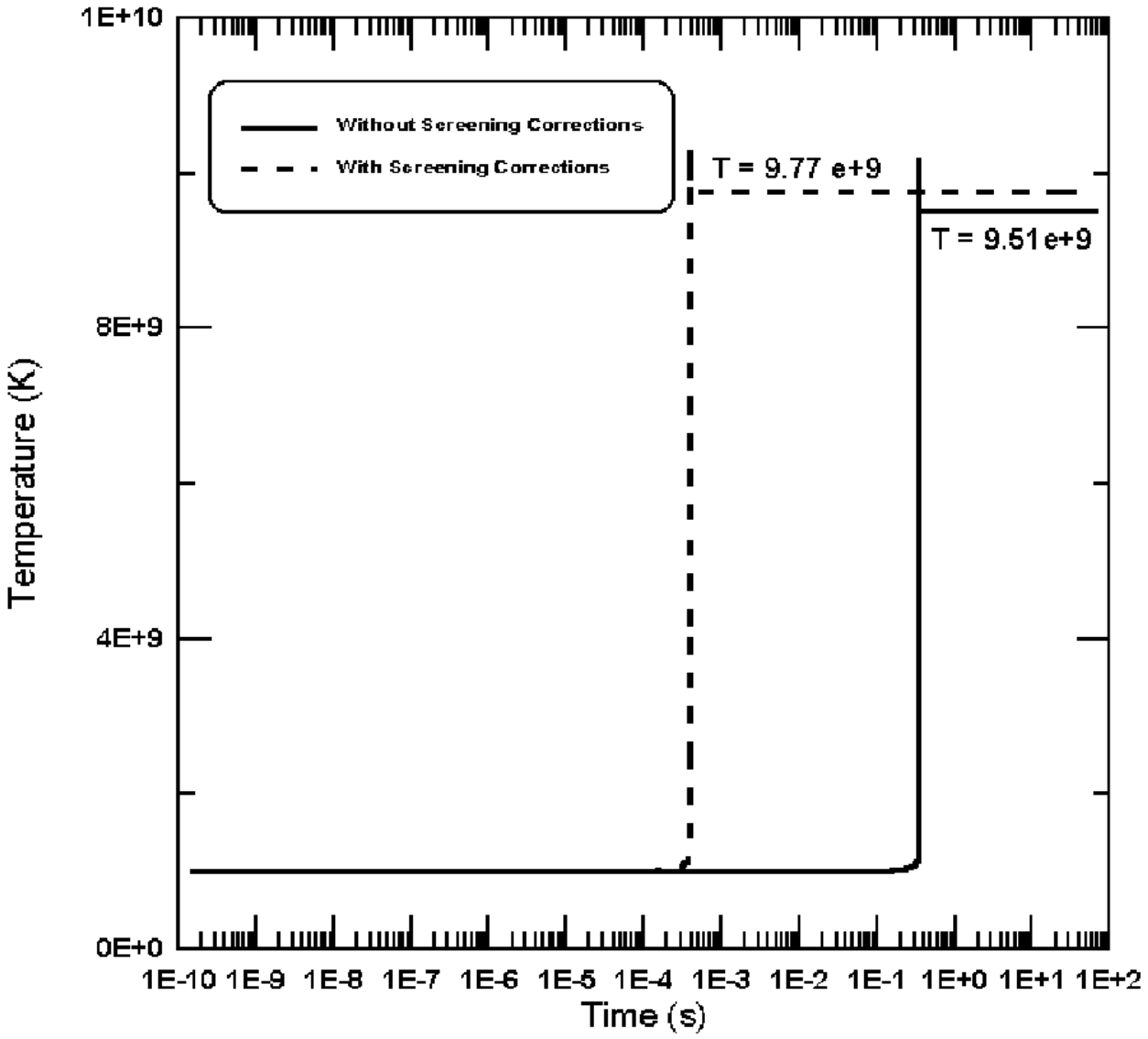

Fig. 5.— Influence of the screening corrections on the evolution of temperature during the isochoric combustion of a 50% mix of carbon and oxygen at $\rho = 4 \times 10^9$ g.cm^{-3}. Inclusion of screening factors (dashed line) led to a higher temperature value during the NSE. (14-isotope chain).

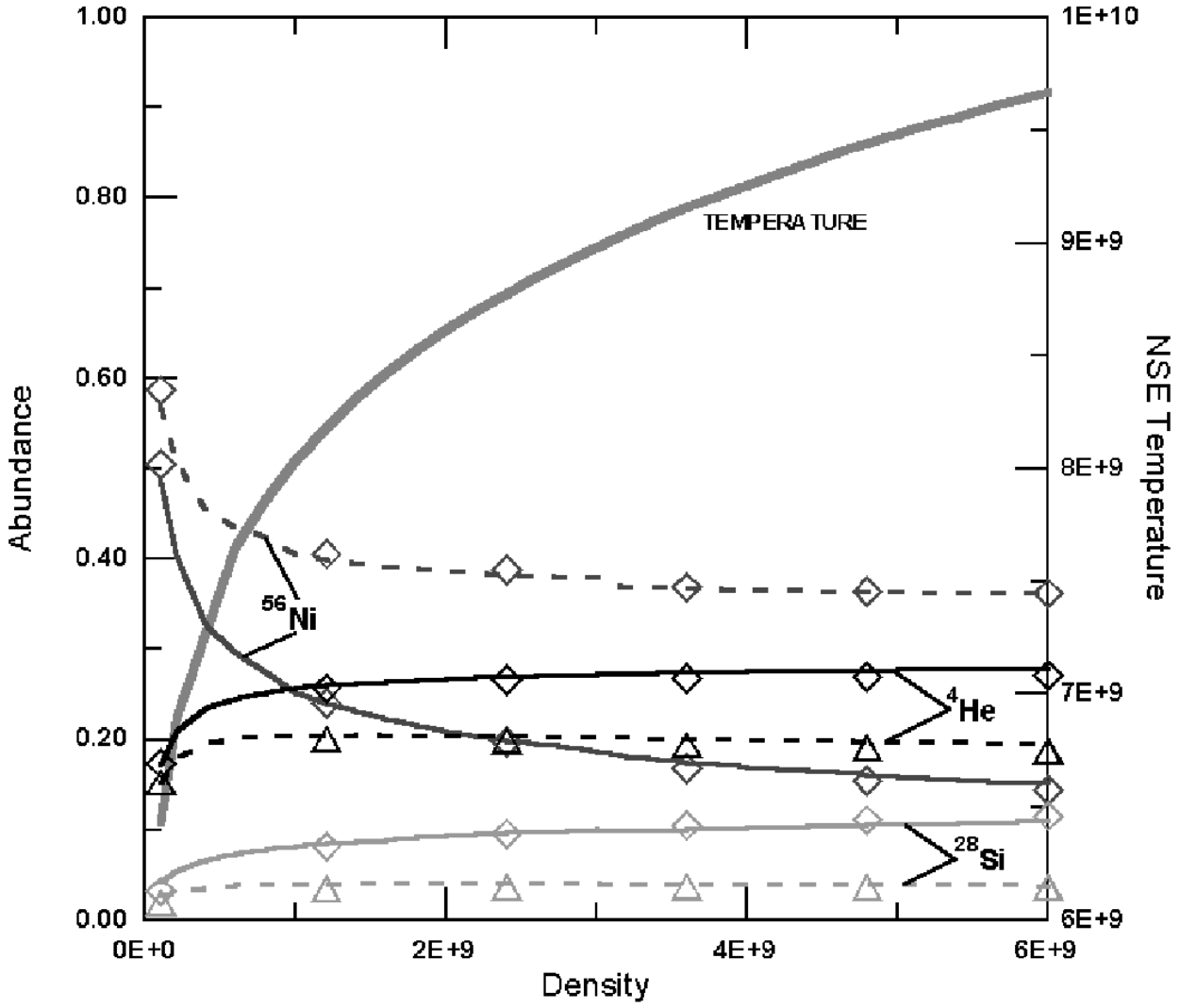

Fig. 6.— Abundance of ^{4}He, ^{28}Si and ^{56}Ni at several densities once the NSE has been achieved. For a given density and temperature the isotopic composition at NSE sensitively depends on the inclusion of the screening corrections to the nuclear reaction rates. Continuum lines depicts the abundances when no screening factors are taken into account. Dashed lines are for the screening factors given by equation (11). A comparison with the mass fractions obtained by solving the nuclear Saha equation for the same number of species (14) is also provided (triangles and diamonds). In this case the electrostatic interactions were taken into account by substracting the chemical potential of the nuclei from their nuclear mass excess. There is a good agreement between both calculations. As expected, the effect of the electrostatic interactions increases with density. (14-isotope chain).

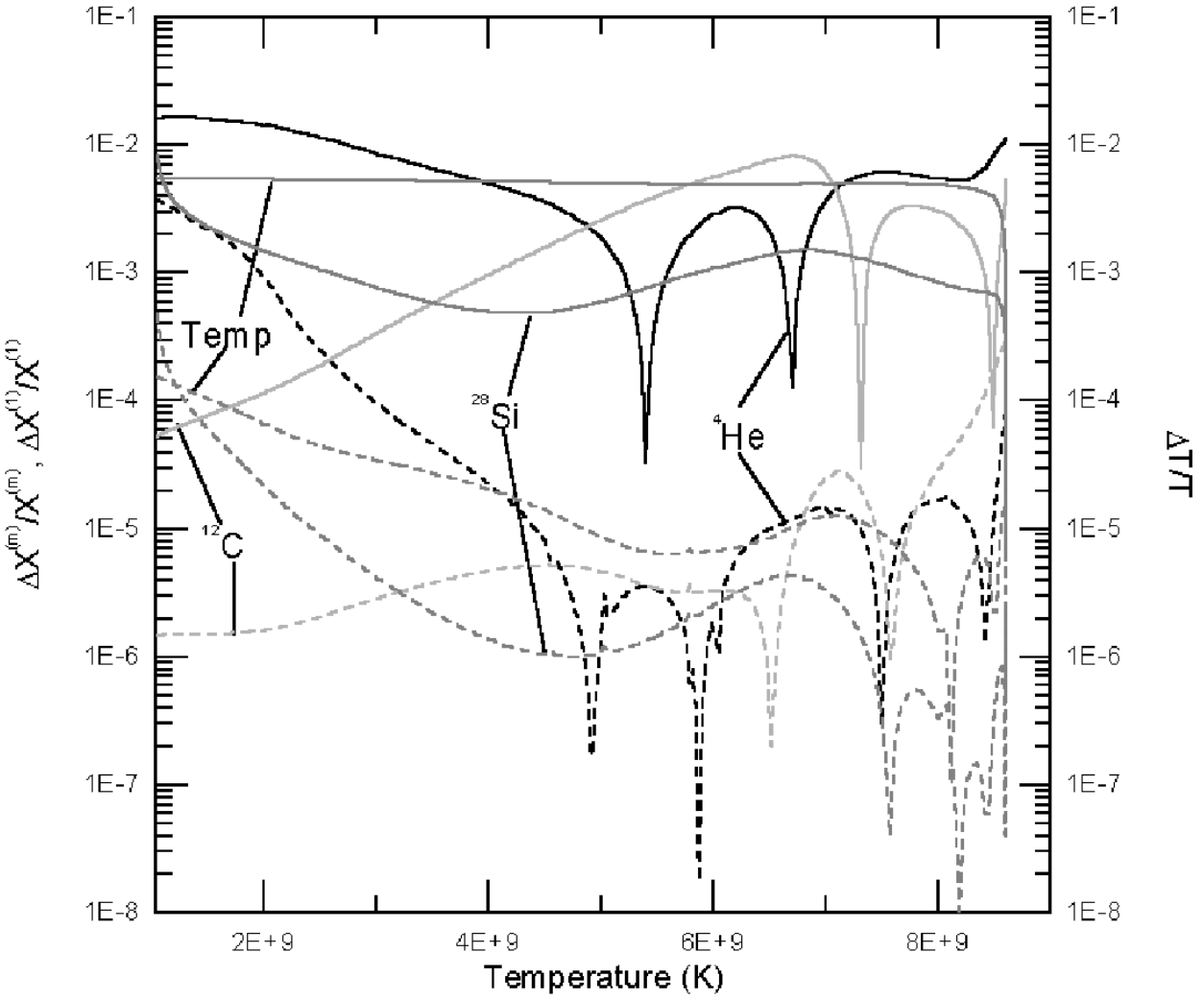

Fig. 7.— Evolution of $\Delta X_i^1/X_i$ (solid lines), and $\sum_k \Delta X_i^k/X_i,\ k = 2, m$ (dashed lines) corresponding to He^4, C^{12} and Si^{28} and the equivalent expressions for temperature, during the isochoric combustion of a 50% mix of carbon and oxygen at $\rho = 10^9$ g.cm^{-3}. Horitzontal axis is temperature, which goes from $T^0 = 10^9$ K to $T = 8.6 \times 10^9$ just before the relaxation to NSE. The error during the purely linear calculation (one iteration) is approximately given by the sum of the higher-order corrections (dashed lines) calculated through the iterative Newton-Raphson scheme described in §3.1.2. The time-step was chosen to allow a relative variation of 1.5% and 10% in temperature and mass-fractions of the more abundant species respectively (86-isotope chain).

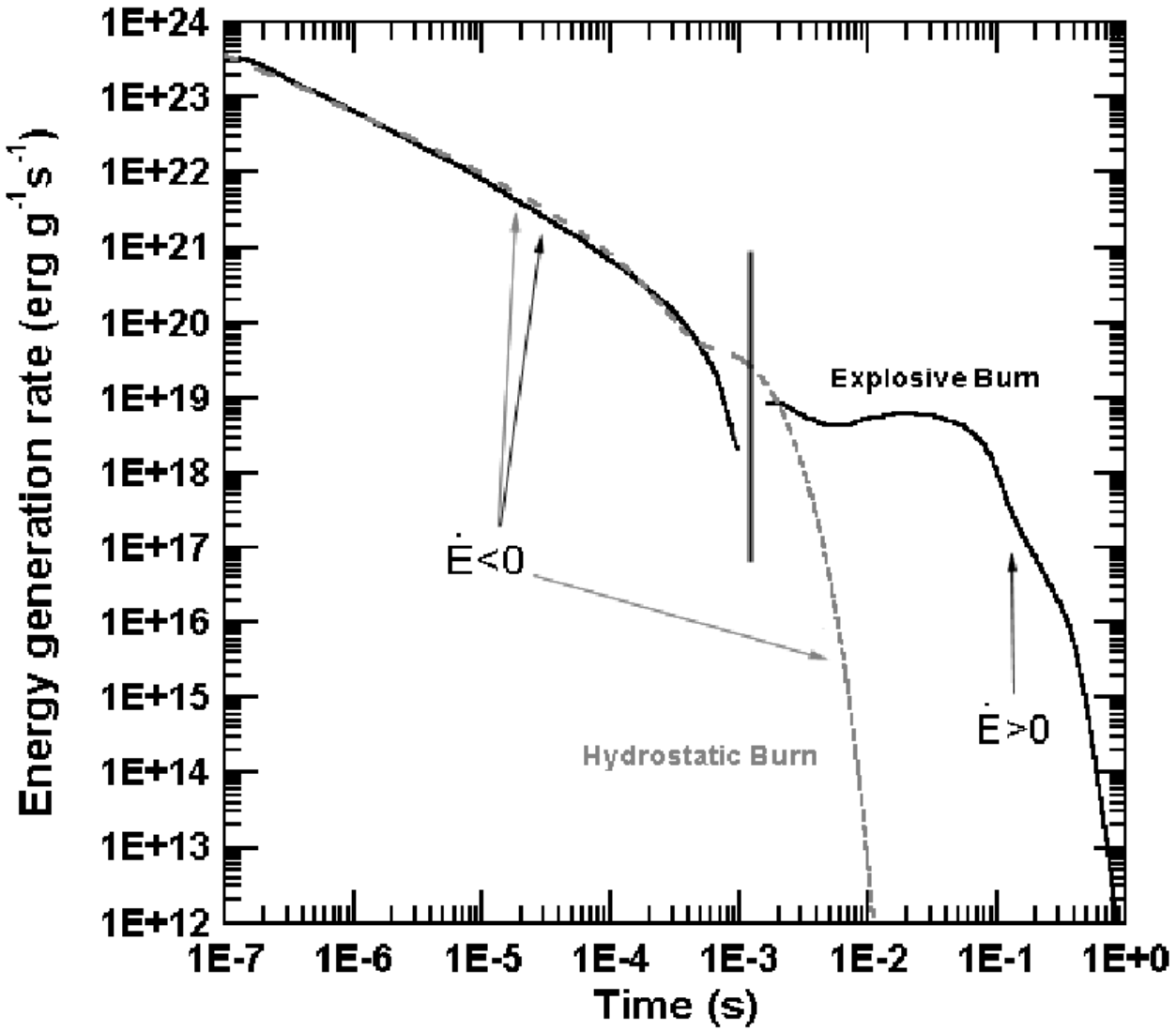

Fig. 8.— Evolution of the nuclear energy generation rate (absolute value) during endoenergetic silicon combustion: at constant density $\rho = 10^7$ g.cm^{-3} and temperature T $= 6 \times 10^9$ K (dashed line), and during the explosive combustion (solid line). For the last case the nuclear energy generation rate becomes positive after 10^{-3} s, (14-isotope chain).

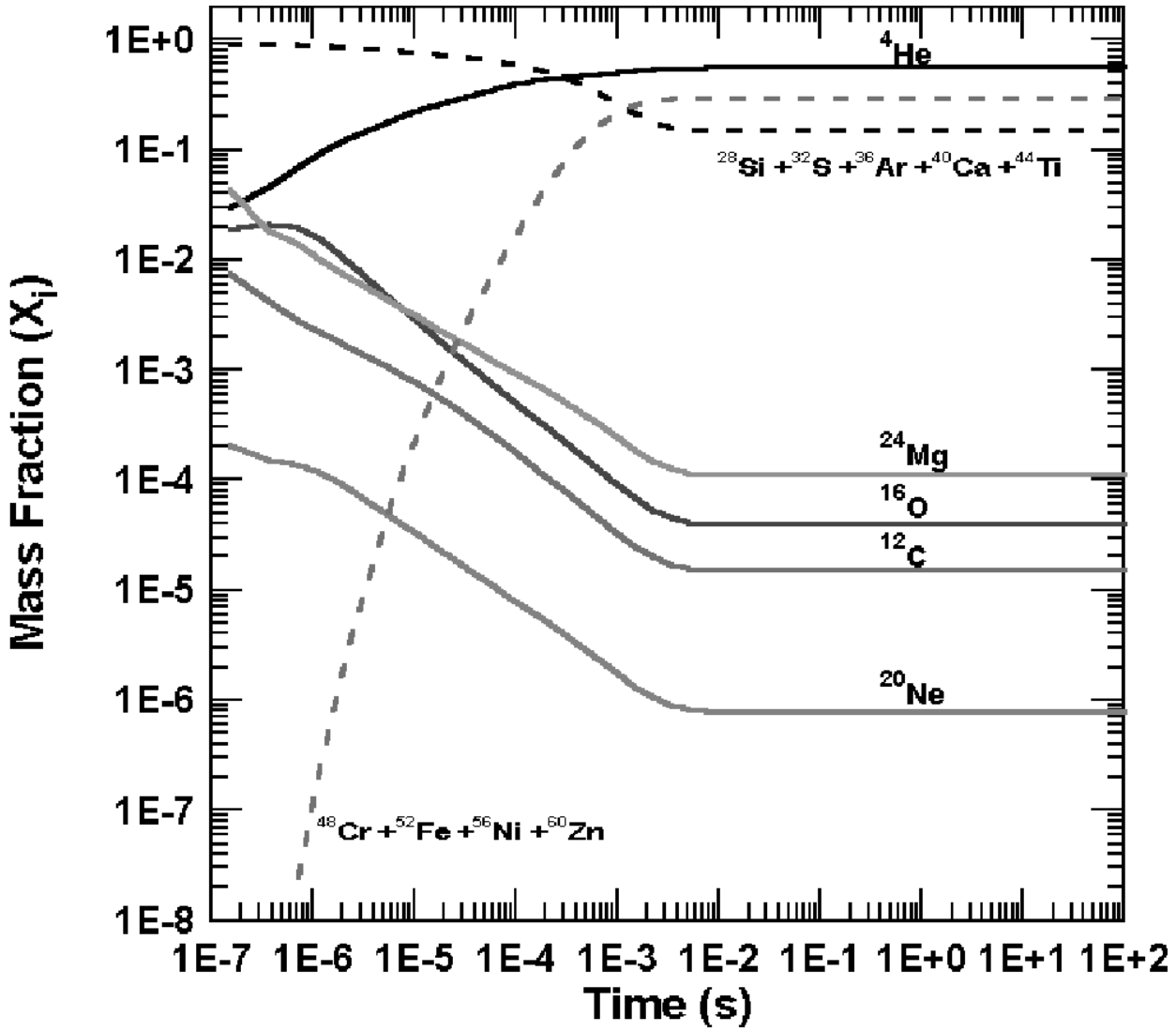

Fig. 9.— The same as Figure 8 but for abundances in the hydrostatic calculation (14-isotope chain).

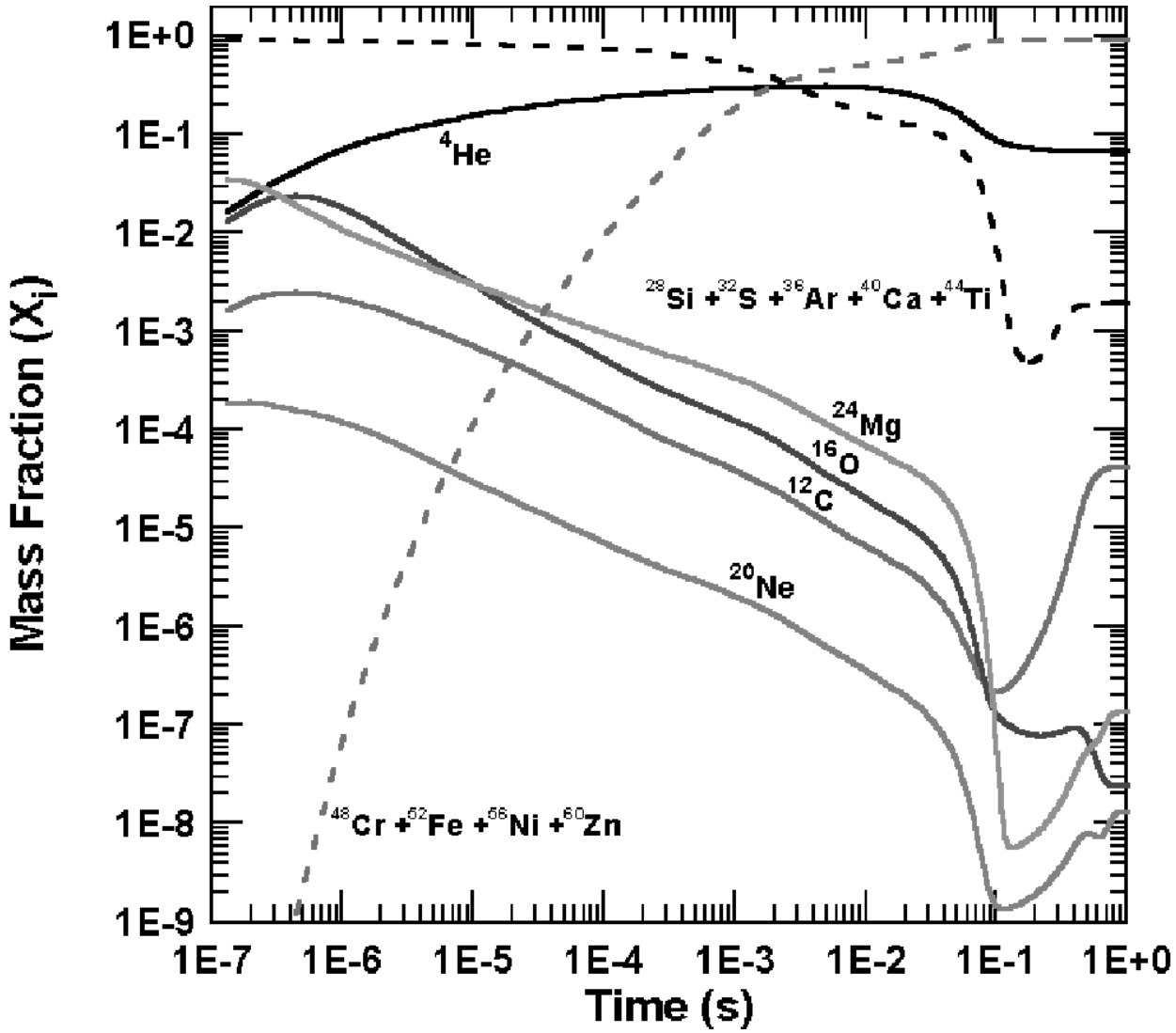

Fig. 10.— The same as in Figure 9 but for the hydrodynamic silicon combustion. Final products are typical of an α-rich freeze out (14-isotope chain).

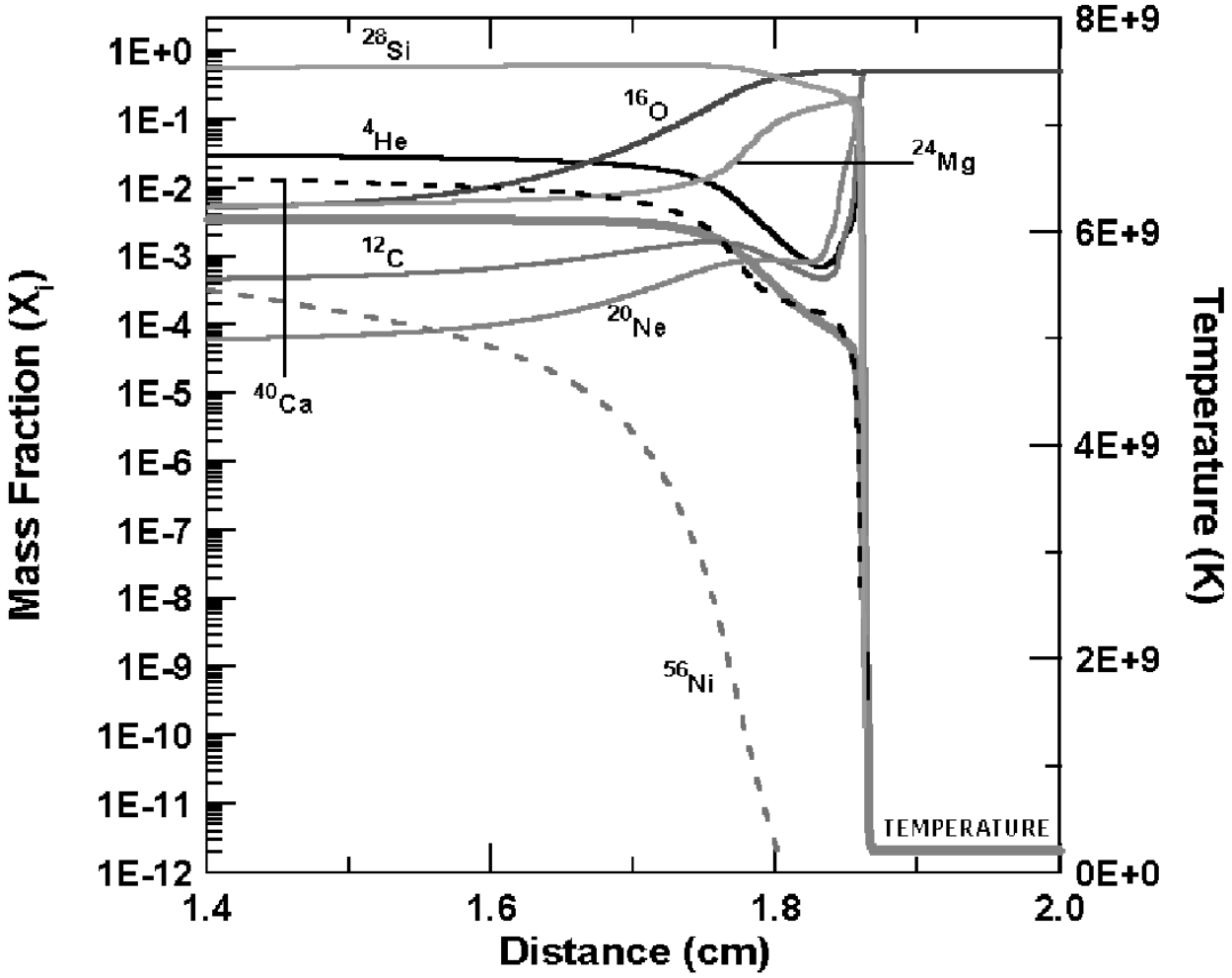

Fig. 11.— Temperature and chemical profiles corresponding to a nuclear flame moving to the right through a medium of density $\rho = 1.26 \times 10^8$ g.cm^{-3} composed of equal parts carbon and oxygen. Again, the feedback between nuclear rates and temperature was adequately handled during the integration, and the relaxation to NSE was smooth (86-isotope network).

Table 1. Abundances during the adiabatic expansion from NSE at $\rho_0 = 10^9$ g.cm^{-3} starting from the NSE temperature $T_0 = 8.03\ 10^9$ K.

Isot.	T_9 : 8.03	4	3.0	2.0	0.5	Isot.	T_9 : 8.03	4.0	3.0	2.0	0.5
n	5.7(-5)	4.8(−12)	3.0(-16)	8.6(-25)	4.0(-85)	^{38}Ca	2.5(-7)	3.1(-14)	2.2(-12)	1.1(-8)	1.3(-8)
p	2.1(-2)	1.7(-3)	5.2(-4)	2.6(-4)	1.6(-6)	^{39}Ca	2.3(-5)	7.1(-12)	2.2(-12)	2.6(-11)	2.6(-11)
^{4}He	1.95(-1)	3.4(-3)	4.5(-3)	4.4(-3)	4.4(-3)	^{40}Ca	5.6(-3)	6.6(-8)	1.3(-7)	4.6(-7)	4.6(-7)
^{12}C	2.5(-5)	1(-8)	1.1(-7)	4.1(-7)	5.1(-7)	^{41}Ca	1.3(-3)	1.7(-11)	1.9(-12)	1.5(-18)	1.3(-21)
^{16}O	5.3(-5)	1.7(-9)	3.2(-9)	1.1(-9)	3.7(-10)	^{42}Ca	7.1(-4)	6.4(-13)	7.6(-15)	1.2(-20)	6.8(-27)
^{20}Ne	3(-6)	3.3(-11)	1.3(-10)	1.6(-11)	4.7(-12)	^{41}Sc	1.5(-5)	4(-12)	4.8(-12)	4.2(-11)	1.8(-10)
^{21}Ne	4.3(-8)	6.2(-17)	2.3(-20)	8.8(-30)	2(-44)	^{42}Sc	5.5(-5)	7.9(-13)	6.6(-13)	3.5(-16)	3(-19)
^{22}Ne	5(-9)	1.4(-19)	2.5(-22)	7.5(-32)	1.3(-65)	^{43}Sc	6.2(-4)	4.6(-12)	1.2(-12)	6.9(-15)	1.9(-17)
^{21}Na	4(-8)	7.7(-14)	6.2(-13)	1.9(-12)	5.1(-12)	^{42}Ti	4.8(-8)	1.1(-14)	8.8(-14)	3.3(-10)	8(-10)
^{22}Na	7.2(-8)	9.4(-15)	3.1(-16)	4.6(-22)	2(-40)	^{43}Ti	1.8(-6)	2.6(-13)	4.8(-12)	8.3(-12)	8.3(-12)
^{23}Na	4.1(-7)	3.1(-14)	5.2(-14)	1.1(-16)	4.3(-25)	^{44}Ti	1.2(-3)	1.3(-8)	6(-8)	7.9(-8)	5.5(-8)
^{22}Mg	1.3(-9)	4.1(-14)	1.4(-11)	4.9(-8)	5.9(-8)	^{45}Ti	1.7(-3)	2.1(-10)	1.4(-12)	5.3(-20)	3.9(-24)
^{23}Mg	1.4(-7)	7.9(-12)	7.8(-11)	7.9(-11)	7.9(-11)	^{46}Ti	4.6(-3)	5.4(-10)	3.9(-13)	2.4(-19)	1.9(-23)
^{24}Mg	1.3(-4)	7.5(-11)	4.2(-10)	1.1(-11)	9.1(-12)	^{45}Va	5.8(-6)	7(-12)	3.3(-11)	3(-10)	1.5(-9)
^{25}Mg	3.9(-6)	7.3(-16)	3.7(-19)	2.6(-29)	1.3(-40)	^{46}Va	1.3(-4)	7.1(-11)	1(-11)	2.4(-15)	2.7(-18)
^{26}Mg	9.1(-7)	1.2(-17)	1.1(-19)	8.4(-29)	2.2(-51)	^{47}Va	4.8((-3)	7.8(-9)	1.7(-10)	6.5(-13)	1.1(-13)
^{25}Al	1.1(-6)	1.1(-13)	1.5(-12)	6.7(-13)	1.2(-11)	^{46}Cr	2.9(-8)	2(-13)	2.2(-11)	1.5(-7)	1.8(-7)
^{26}Al	4.2(-6)	4.7(-14)	1.7(-15)	2.9(-21)	1.8(-32)	^{47}Cr	7.9(-6)	5.7(-11)	2.5(-10)	2.6(-10)	2.6(-10)
^{27}Al	4.5(-6)	6.9(-13)	3.6(-12)	7.8(-15)	2.8(-17)	^{48}Cr	4(-3)	4.3(-6)	2.2(-7)	2(-7)	5.7(-8)
^{26}Si	3.1(-8)	5.3(-14)	2.3(-11)	3.4(-8)	3.5(-8)	^{49}Cr	1.2(-2)	6.9(-7)	2.1(-9)	2.8(-16)	2.6(-19)
^{27}Si	5.3(-6)	2(-11)	2(-10)	2(-10)	2(-10)	^{50}Cr	5.2(-2)	2(-6)	1.6(-12)	5.7(-20)	7.3(-24)
^{28}Si	8.9(-3)	5(-10)	3.3(-9)	3.6(-11)	1(-12)	^{49}Mn	2.2(-5)	3.9(-9)	3.4(-10)	5.4(-9)	3.5(-9)
^{29}Si	6(-4)	4.5(-14)	9.7(-19)	1.4(-25)	1.7(-34)	^{50}Mn	7.5(-4)	1.3(-7)	5.7(-9)	1.2(-12)	7.1(-15)
^{30}Si	1.7(-4)	5.3(-16)	1.1(-17)	1.3(-26)	7.1(-42)	^{51}Mn	3.1(-2)	2.1(-5)	6.2(-10)	1.8(-13)	1.3(-14)
^{29}P	6.5(-5)	9.8(-13)	1.8(-11)	1.3(-11)	2.5(-12)	^{50}Fe	1.3(-7)	2.5(-11)	2.4(-11)	3.3(-7)	4.8(-7)
^{30}P	2.2(-4)	3(-13)	2.7(-14)	6(-19)	7.1(-27)	^{51}Fe	3.6(-5)	7.3(-8)	8.6(-8)	9.4(-8)	9.4(-8)
^{31}P	9.2(-4)	6.2(-13)	2.8(-12)	1.4(-15)	3.1(-19)	^{52}Fe	1.3(-2)	2.1(-3)	8.9(-6)	7.6(-6)	7.5(-6)
^{30}S	9.2(-7)	5.6(-14)	1.5(-11)	1.6(-8)	1.7(-8)	^{53}Fe	5.1(-2)	4.1(-4)	1.6(-5)	7.7(-12)	6.8(-14)
^{31}S	4.6(-5)	3.3(-12)	2.4(-11)	2.4(-11)	2.4(-11)	^{54}Fe	2.7(-1)	3(-3)	5.5(-7)	3.6(-16)	8.4(-20)
^{32}S	8.8(-3)	1.2(-9)	1.1(-8)	2.7(-10)	2.6(-12)	^{53}Co	2.5(-5)	4.1(-7)	2(-9)	1.3(-8)	1.3(-8)
^{33}S	1.5(-3)	3.6(-13)	1.8(-15)	1(-23)	1.4(-30)	^{54}Co	2.1(-3)	4.8(-5)	2.3(-5)	1(-8)	3.4(-10)
^{34}S	7.6(-4)	2.1(-14)	1.5(-15)	2.5(-23)	1(-34)	^{55}Co	9.6(-2)	1.9(-2)	9.9(-5)	3.7(-10)	8.4(-12)
^{33}Cl	6.5(-5)	1.2(-12)	2(-11)	1.3(-11)	1.8(-12)	^{54}Ni	7.8(-8)	1.3(-9)	5.2(-11)	1.2(-7)	2.3(-7)
^{34}Cl	3.2(-4)	6.1(-13)	7.7(-14)	2.1(-18)	1.1(-25)	^{55}Ni	5.3(-5)	9.1(-6)	8.9(-5)	1.3(-4)	1.3(-4)
^{35}Cl	1.9(-3)	3.1(-14)	2.1(-11)	2.5(-14)	2.8(-17)	^{56}Ni	2.3(-2)	9.18(-1)	9.65(-1)	9.63(-1)	9.63(-1)
^{34}Ar	8(-7)	7.4(-14)	2.3(-11)	3.6(-8)	3.6(-8)	^{57}Ni	5.5(-2)	3.4(-2)	2.7(-2)	1.8(-2)	1(-2)
^{35}Ar	4.5(-5)	3.4(-12)	3(-11)	3.1(-11)	3.1(-11)	^{58}Ni	1.14(-1)	1.8(-2)	1.4(-3)	1.6(-8)	7.2(-10)
^{36}Ar	6.3(-3)	2.2(-9)	8.2(-9)	2.94(-9)	7.9(-10)	^{57}Cu	2.2(-5)	9.5(-6)	3.9(-6)	4.7(-6)	5.3(-6)
^{37}Ar	1.3(-3)	1(-12)	2.6(-15)	1.9(-23)	2.74(-29)	^{58}Cu	5(-4)	6.2(-5)	1.4(-4)	6.2(-3)	6.8(-3)
^{38}Ar	1.1(-3)	1.9(-13)	5.4(-15)	8(-22)	6.5(-30)	^{59}Cu	5.4(-3)	6(-4)	2.4(-4)	5.8(-7)	1.7(-7)
^{37}K	2.8(-5)	6.8(-13)	3(-12)	1.2(-11)	7.1(-11)	^{58}Zn	1.2(-8)	6(-10)	4.5(-10)	1.4(-8)	2.7(-9)
^{38}K	2.3(-4)	2.3(-12)	1.6(-13)	7(-18)	1.1(-22)	^{59}Zn	1.8(-6)	8.7(-8)	6.7(-7)	2.8(-3)	1.02(-2)
^{39}K	2.3(-4)	3.1(-11)	7.9(-11)	8.5(-13)	1.1(-13)	^{60}Zn	1.3(-4)	1.5(-4)	1.7(-3)	4.9(-3)	4.9(-3)

Table 2. Five more abundant nuclei at NSE and at the freeze-out temperature for the models considered in Sec. 3.1. The NSE temperature and mass fractions of these nuclei are given in the left side of the Table, as a function of the initial composition of the fuel. The approximate freeze out temperature and the corresponding abundances are also given in the right part of the Table. A specie is considered burned once its mass fraction differs from its final stable value in less than 2%. Temperatures are in units of 10^9 K.

Fuel		NSE					FREEZE OUT				
	Ash	^{54}Fe	^{4}He	^{58}Ni	^{55}Co	^{57}Ni	^{56}Ni	^{59}Zn	^{57}Ni	^{58}Cu	^{60}Zn
CO	X_k	2.7(−1)	1.95(−1)	1.14(−1)	9.55(−2)	5.46(−2)	9.63(−1)	1.02(−2)	1.01(−2)	6.82(−3)	4.93(−3)
	T_9	8.03	8.03	8.03	8.03	8.03	3.20	1.31	1.37	1.35	2.10
	Ash	^{54}Fe	^{4}He	^{50}Cr	^{58}Ni	^{34}S	^{54}Fe	^{58}Ni	^{50}Cr	^{4}He	^{46}Ti
CONe	X_k	4.1(−1)	1.99(−1)	1.59(−1)	1.04(−1)	3.08(−2)	7.25(−1)	2.12(−1)	5.58(−2)	9.49(−3)	3.11(−3)
	T_9	8.51	8.51	8.51	8.51	8.51	5.52	4.77	4.75	4.45	4.63
	Ash	^{56}Ni	^{55}Co	^{54}Fe	^{57}Ni	^{58}Ni	^{56}Ni	^{57}Ni	^{59}Zn	^{58}Cu	^{4}He
He	X_k	6.2(−1)	1.1(−1)	9.3(−2)	5.0(−2)	3.8(−2)	9.7(−1)	8.2(−3)	6.5(−3)	4.3(−3)	1.7(−3)
	T_9	4.30	4.32	4.32	4.32	4.32	2.95	1.14	1.11	1.23	2.43